

EvoVGM: A Deep Variational Generative Model for Evolutionary Parameter Estimation

Amine M. Remita

remita.amine@courrier.uqam.ca
 Department of Computer Science
 Université du Québec à Montréal
 Montréal, Québec, Canada

Abdoulaye Baniré Diallo

diallo.abdoulaye@uqam.ca
 Department of Computer Science
 Université du Québec à Montréal
 Montréal, Québec, Canada

ABSTRACT

Most evolutionary-oriented deep generative models do not explicitly consider the underlying evolutionary dynamics of biological sequences as it is performed within the Bayesian phylogenetic inference framework. In this study, we propose a method for a deep variational Bayesian generative model that jointly approximates the true posterior of local biological evolutionary parameters and generates sequence alignments. Moreover, it is instantiated and tuned for continuous-time Markov chain substitution models such as JC69 and GTR. We train the model via a low-variance variational objective function and a gradient ascent algorithm. Here, we show the consistency and effectiveness of the method on synthetic sequence alignments simulated with several evolutionary scenarios and on a real virus sequence alignment.

KEYWORDS

Variational Generative Model, Evolutionary model, Substitution model, Variational inference, Latent variables, Deep Neural networks

1 INTRODUCTION

In systematics and evolutionary biology, probabilistic evolutionary models are extensively used to study unseen and complex historical events affecting the genomes of a set of taxa during a period of time (i.e. recombination, horizontal gene transfer, selective pressure etc.). Their ability to detect and measure evolutionary events using biological sequences has enabled valuable applications in population genetics [12], medicine [31] and epidemiology [4, 5]. These models allow the estimation of probabilities of certain types of mutations such as substitutions [10, 25], indels [3] and genome rearrangements [21]. Main approaches supporting evolutionary studies, such as phylogenetics, implement evolutionary models with Markovian properties [25].

Typically, evolutionary parameters of these models are jointly represented with different types of high-dimensional variables (discrete and continuous), inducing a computationally intractable joint posterior. Bayesian phylogenetic approaches provide methods to efficiently approximate the intractable joint posterior and quantify the uncertainty in the estimation of the parameters [8, 30]. They mainly implement random-walk Markov Chain Monte Carlo (MCMC) algorithms, which can converge to an accurate posterior but with a considerable cost. Furthermore, they are prone to limitations due to the complexity of the posterior [27], their dependence on initialization and proposal distribution parameters, and their sensitivity to the prior distributions [7]. Recently, variational inference (VI) has sparked interest in phylogenetics as a robust alternative

to approximate the intractable posterior by relying on fast optimization methods [2, 9, 32]. VI finds an optimal candidate from a space of tractable distributions that minimizes the Kullback-Leibler (KL) divergence to the exact posterior [2, 9]. Additionally, it inherently bounds the intractable marginal likelihood of the observed data. Moreover, VI is also used in building deep generative models [15, 19]. However, contrary to Bayesian phylogenetic inference frameworks, most evolutionary-oriented deep generative models do not explicitly consider the underlying evolutionary dynamics of the biological sequences [1, 22, 26].

Here, we propose evoVGM, a deep variational generative model that simultaneously estimates local evolutionary parameters and generates nucleotide sequence data. Like phylogenetic inference, we explicitly integrate a continuous-time Markov chain substitution model into the generative model like phylogenetic inference. The new method is trained in an unsupervised manner following the evolutionary model constraints.

2 BACKGROUND

2.1 Notation

The observed data \mathbf{X} is an alignment of M character sequences with length N where $\mathbf{X} \in \mathcal{A}^{M \times N}$. In our case the alphabet of characters $\mathcal{A} = \{A, G, C, T\}$ is a set of nucleotides. x_n^m is the character in the m^{th} sequence (x^m) and at the n^{th} site (x_n) of the alignment. We assume each alignment \mathbf{X} has a hidden ancestral state sequence $\mathbf{a} \in \mathcal{A}^N$. Each ancestral state a_n would have evolved, independently from other states $\{a_i; i \neq n\}$, to an extant character x_n^m over an evolutionary time expressed as a branch length b and following a substitution model defined by a set of parameters ψ . In a Bayesian framework, we seek representations allowing to model uncertainty on the quantity and composition of different entities. Here, we consider the observable characters (x_n^m) and the ancestral states (\mathbf{a}_n) as random variables and represent them by categorical distributions over \mathcal{A} . Also, branch lengths (\mathbf{b}^m) and substitution model parameters (ψ) will be modelled as random variables.

2.2 Markov Chain Models of Character Substitution

The evolution of a character is measured by the number of hidden substitutions that undergoes over time. To estimate this quantity, we assume that the process of evolution follows a continuous-time Markov chain model whose states belong to \mathcal{A} . The model is parameterized by a rate matrix \mathbf{Q} and relative frequencies π of characters at equilibrium. Each element of the matrix q_{ij} ($i \neq j$) defines the instantaneous substitution rate of character i changing into character j . The diagonal elements q_{ii} are set up in a way

that each row sums to 0. \mathbf{Q} is scaled by factor β so that the time b will be measured in expected number of substitutions per site and the average rate of substitution at equilibrium will be 1. We use time-reversible Markov chain models assuming the amount of changes from one character to another is the same in both ways. For nucleotide substitution time-reversible models, the equation of \mathbf{Q} is

$$\mathbf{Q} = \begin{pmatrix} \cdot & a\pi_G & b\pi_C & c\pi_T \\ a\pi_A & \cdot & d\pi_C & e\pi_T \\ b\pi_A & d\pi_G & \cdot & f\pi_T \\ c\pi_A & e\pi_G & f\pi_C & \cdot \end{pmatrix} \beta,$$

where $a, b, c, d, e,$ and f are the set of relative substitution rate parameters ρ , and $\pi_A + \pi_G + \pi_C + \pi_T = 1$ are the relative frequencies π . Once \mathbf{Q} is estimated we can compute the probability transition matrix \mathbf{P} over evolutionary time b as $\mathbf{P}(b) = \exp(\mathbf{Q} b)$. The matrix exponential is computed using spectral decomposition of \mathbf{Q} as it is reversible. $\mathbf{P}(b) = \mathbf{U} \text{diag}\{\eta_0, \eta_1, \eta_2, \eta_3\} \mathbf{U}^{-1}$ where $\eta_i = \exp(\lambda_i b)$, λ_i are the eigenvalues of \mathbf{Q} , \mathbf{U} is the matrix of eigenvectors and \mathbf{U}^{-1} is its inverse. (see [16] and [29] for more details.)

Different substitution models could be generated depending on the constraints placed on the set of parameters $\psi = \{\rho, \pi\}$. The simplest model is JC69, having equal substitution rates and uniform relative frequencies [10]. The K80 defines uniform frequencies as JC69. However, it differentiates between the two types of substitution rates corresponding to transitions ($\alpha = a = f$) and transversions $\beta = b = c = d = e$ [13]. Usually, K80 is parameterized by the transition/transversion rate ratio $\kappa = \alpha/\beta$. Finally, the general time-reversible (GTR) model sets all the parameters ψ free [25, 28].

2.3 Evolutionary Posterior

Along with \mathbf{a} and \mathbf{b} variables, we consider the parameters of the Markov chain model ψ as latent (hidden) variables to be inferred from the observed data. Assuming an independent evolution of sites in a sequence [6], the marginal likelihood of the observed data is $p(\mathbf{X}) = \prod_{n=1}^N p(\mathbf{x}_n)$. The inference of the latent variables for each site \mathbf{x}_n requires computation of the joint posterior probability using Bayes' theorem:

$$p(\mathbf{a}_n, \mathbf{b}, \psi | \mathbf{x}_n) = \frac{p(\mathbf{x}_n, \mathbf{a}_n, \mathbf{b}, \psi)}{p(\mathbf{x}_n)}. \quad (1)$$

This exposes the joint density of the observable and the latent variables $p(\mathbf{x}_n, \mathbf{a}_n, \mathbf{b}, \psi)$, and the marginal likelihood $p(\mathbf{x}_n)$. The former is factorized into the likelihood and the prior density of latent variables $p(\mathbf{x}_n | \mathbf{a}_n, \mathbf{b}, \psi) p(\mathbf{a}_n, \mathbf{b}, \psi)$. The latter is calculated by marginalizing over the values of all the latent variables as $\iiint p(\mathbf{x}_n | \mathbf{a}_n, \mathbf{b}, \psi) p(\mathbf{a}_n, \mathbf{b}, \psi) d\mathbf{a}_n d\mathbf{b} d\psi$. The computation of the evolutionary joint posterior density is computationally intractable as it depends on the evaluation of $p(\mathbf{x}_n)$ which is intractable due to the integrals in its marginalization. We show in the next section strategies to determine each term in the equation 1.

3 PROPOSED EVOLUTIONARY MODEL

In this section, we describe a deep variational generative model that simultaneously estimates local evolutionary biological parameters and generates nucleotide sequence data. Similar to deep variational-based generative models [15, 19], the proposed model architecture

consists of two main sub-models: 1) a set of deep variational encoders that infer the parameters of evolutionary-latent-variable distributions and allow sampling, and 2) a generating model that computes probability transition matrices from sampled latent variables and generates a distribution of sequence alignments from reconstructed ancestral states (see Figure 1).

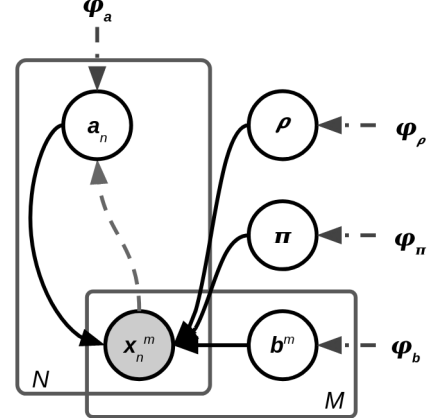


Figure 1: Graphical illustration of inference (dashed gray lines) and generation (solid lines) processes of the GTR-based variational generative model. ϕ are the set of hyper-priors. Gray circles are observed variables. Blank circles are latent variables.

3.1 Variational Inference of the Joint Posterior

We use variational inference to approximate the true joint posterior probability distribution by a new probability distribution $q_{\phi}(\mathbf{a}_n, \mathbf{b}^m, \psi | \mathbf{x}_n)$ [9, 15, 19]. The approximate distributions of the latent variables will be modelled using non-linear transformations parameterized by the set of independent variational parameters $\phi = \{\phi_a, \phi_b, \phi_{\psi}\}$, which are *adaptable* and *individually shared across the sites \mathbf{x}_n* .

An ancestral variable \mathbf{a}_n is inferred and sampled for each alignment site \mathbf{x}_n with an approximate density $q_{\phi_a}(\mathbf{a}_n | \mathbf{x}_n)$ represented by a categorical distribution over the $(|\mathcal{A}| - 1)$ -simplex. We apply a non-linear transformation on \mathbf{x}_n to produce the local parameters of $q_{\phi_a}(\mathbf{a}_n | \mathbf{x}_n)$ which are a set of $|\mathcal{A}|$ probabilities summing to one as

$$q_{\phi_a}(\mathbf{a}_n | \mathbf{x}_n) = \text{Categorical}(\mathbf{a}_n; \text{NeuralNet}(\mathbf{x}_n; \phi_a)),$$

where $\text{NeuralNet}(\cdot; \phi_a)$ function denotes a deep neural network being the non-linear transformation parameterized by ϕ_a with a softmax(\cdot) function for its last layer.

For each sequence \mathbf{x}^m , an evolutionary time variable \mathbf{b}^m will be inferred. We model its approximate density $q_{\phi_b}(\mathbf{b}^m)$ using a gamma distribution to ensure the positiveness of the samples. The parameters of the distribution (shape and rate) are produced by a non-linear transformation as follows:

$$q_{\phi_b}(\mathbf{b}^m) = \text{Gamma}(\mathbf{b}^m; \text{NeuralNet}(\phi_b)).$$

Lastly, we infer the latent variables of the Markov chain model parameters ψ with independent approximate densities $q_{\phi_{\psi}}(\psi)$. The

JC69 model does not have any free parameters to be estimated ($\psi = \emptyset$). For the K80 model, we infer the latent variable of the transition/transversion rate ratio (κ) using a gamma-based approximate distribution ($q_{\phi_\kappa}(\kappa)$), which its parameters are produced by a neural network:

$$q_{\phi_\kappa}(\kappa) = \text{Gamma}(\kappa; \text{NeuralNet}(\phi_\kappa)).$$

In the case of the GTR model, we model the variational densities of the substitution rate parameters (ρ) and the relative frequencies (π) using Dirichlet distributions. This ensures that the sum of the sampled values is equal to one. Their concentrations are generated by a set of independent neural networks parameterized by ϕ_ρ and ϕ_π , respectively:

$$\begin{aligned} q_{\phi_\rho}(\rho) &= \text{Dirichlet}(\rho; \text{NeuralNet}(\phi_\rho)), \\ q_{\phi_\pi}(\pi) &= \text{Dirichlet}(\pi; \text{NeuralNet}(\phi_\pi)). \end{aligned}$$

Using a mean-field variational inference approach, the approximate joint posterior factorizes into:

$$q_\phi(\mathbf{a}_n, \mathbf{b}, \psi | \mathbf{x}_n) = q_{\phi_a}(\mathbf{a}_n | \mathbf{x}_n) \prod_{m=1}^M q_{\phi_b}(\mathbf{b}^m) q_{\phi_\psi}(\psi). \quad (2)$$

3.2 Generating Model Computation

The generating model represented by the joint density $p(\mathbf{x}_n, \mathbf{a}_n, \mathbf{b}^m, \psi)$ which is parameterized only by local latent variables. We use independent prior densities for the latent variables $p(\mathbf{a}_n, \mathbf{b}^m, \psi) = p(\mathbf{a}) p(\mathbf{b}) p(\psi)$. To ease the computation, for each prior density we applied the same distribution type as its corresponding approximate density of the posterior. Moreover, for each nucleotide x_n^m , we use the probability transition matrix $\mathbf{P}(\mathbf{b}^m)$ to define the likelihood function which is the probability of evolving a character \mathbf{a}_n into \mathbf{x}_n^m during a time \mathbf{b}^m .

$$\begin{aligned} \widehat{\mathbf{x}}_n^m &= \mathbf{a}_n \times \mathbf{P}(\mathbf{b}^m; \psi), \\ p(\mathbf{x}_n^m | \mathbf{a}_n, \mathbf{b}^m, \psi) &= \text{Categorical}(\mathbf{x}_n^m; \widehat{\mathbf{x}}_n^m). \end{aligned} \quad (3)$$

The likelihood is computed following a pre-order traversal. We call it a top-down likelihood, since it includes sampled ancestral states in its estimation. It is different from the likelihood computed in a phylogeny, which is based on a post-order traversal [6] and does not include sampled ancestral states. Finally, the joint density is

$$\begin{aligned} p(\mathbf{x}_n, \mathbf{a}_n, \mathbf{b}, \psi) &= p(\mathbf{a}) p(\mathbf{b}) p(\psi) \\ &\prod_{m=1}^M p(\mathbf{x}_n^m | \mathbf{a}, \mathbf{b}^m, \psi). \end{aligned} \quad (4)$$

3.3 Stochastic Estimator and Learning Algorithm

Variational inference allows us to form a lower bound on the marginal likelihood of each site $\log p(\mathbf{x}_n) \geq \mathcal{L}_n(\phi, \mathbf{x}_n)$, where \mathcal{L}_n is the evidence lower bound (ELBO) [2, 9]. Putting together equations 1, 2 and 4, we can derive the equation of the multi-sample estimator

of the EvoVGM model as follows:

$$\begin{aligned} \mathcal{L}_n(\phi, \mathbf{x}_n) &= \left(\frac{1}{L} \sum_{l=1}^L \sum_{m=1}^M \log p(\mathbf{x}_n^m | \mathbf{a}_n^l, \mathbf{b}^{m,l}, \psi^l) \right) \\ &- \alpha_{\text{KL}} \left(\text{KL}(q_{\phi_a}(\mathbf{a}_n | \mathbf{x}_n) \| p(\mathbf{a})) + \sum_{m=1}^M \text{KL}(q_{\phi_b}(\mathbf{b}^m) \| p(\mathbf{b})) \right. \\ &\quad \left. + \text{KL}(q_{\phi_\psi}(\psi) \| p(\psi)) \right), \end{aligned}$$

where L is the sampling size, $\text{KL}(\cdot \| \cdot)$ is the Kullback–Leibler divergence, and α_{KL} is a regularization coefficient (see the development of this equation in A.1). This estimator is computationally tractable because it is independent of the direct evaluation of the true joint posterior. To maximize the ELBO and learn the global variational parameters ϕ , EvoVGM estimates and backpropagates the gradients for the whole data \mathbf{X} using the reparameterization trick [15] and a gradient ascent optimizer. The algorithm of EvoVGM is detailed in 1 section. It is implemented in Pytorch [18] and its open-source code is available at <https://github.com/maremita/evoVGM>.

Algorithm 1 Learning algorithm for EvoVGM

Input: \mathbf{X}

$\phi_a, \phi_b, \phi_\psi \leftarrow$ initialize global variational parameters

for $i \in [1 \dots \text{max_iter}]$ **do**

$\mathbf{b}^m \leftarrow$ Sample $M \times L$ branch latent variables (ϕ_b)

$\psi \leftarrow$ Sample L evolutionary latent variables (ϕ_ψ)

$\mathbf{P}^m \leftarrow$ Compute $M \times L$ probability transition matrices (\mathbf{b}^m, ψ)

for $n \in [1 \dots N]$ **do**

$\mathbf{a}_n \leftarrow$ Sample L ancestor latent variable ($\mathbf{x}_n; \phi_a$)

$\widehat{\mathbf{x}}_n \leftarrow$ Generate $M \times L$ nucleotides ($\mathbf{a}_n, \mathbf{P}^m$)

$\mathcal{L}_n \leftarrow$ Compute ELBO according to equation A.1

$\mathcal{L} += \mathcal{L}_n$

end for

$\mathbf{g} \leftarrow$ Compute gradients of total ELBO (\mathcal{L})

$\phi_a, \phi_b, \phi_\psi \leftarrow$ Update parameters (\mathbf{g}) with Gradient Ascent optimizer

end for

4 EXPERIMENTS

The evaluation of the proposed Bayesian variational model to estimate evolutionary parameters and generate sequence alignments is oriented towards assessing its consistency, effectiveness, and understanding its behavior during the training using simulated sequence alignments. Moreover, we highlight the robustness of a fine-tuned EvoVGM model by applying it on a sequence alignment of gene S of coronaviruses.

Sequence Alignment Simulation. We used Pyvolve [23] to simulate the evolution of different sequence alignments with a site-wise homogeneity model and a combination of substitution models (JC69, K80 and GTR), the number of sequences (3, 4 and 5) and alignment lengths (100 bp, 1000 bp and 5000 bp). A site-wise homogeneity model evolves sequences from a root sequence with the same substitution model over lineages and with the same branch lengths for

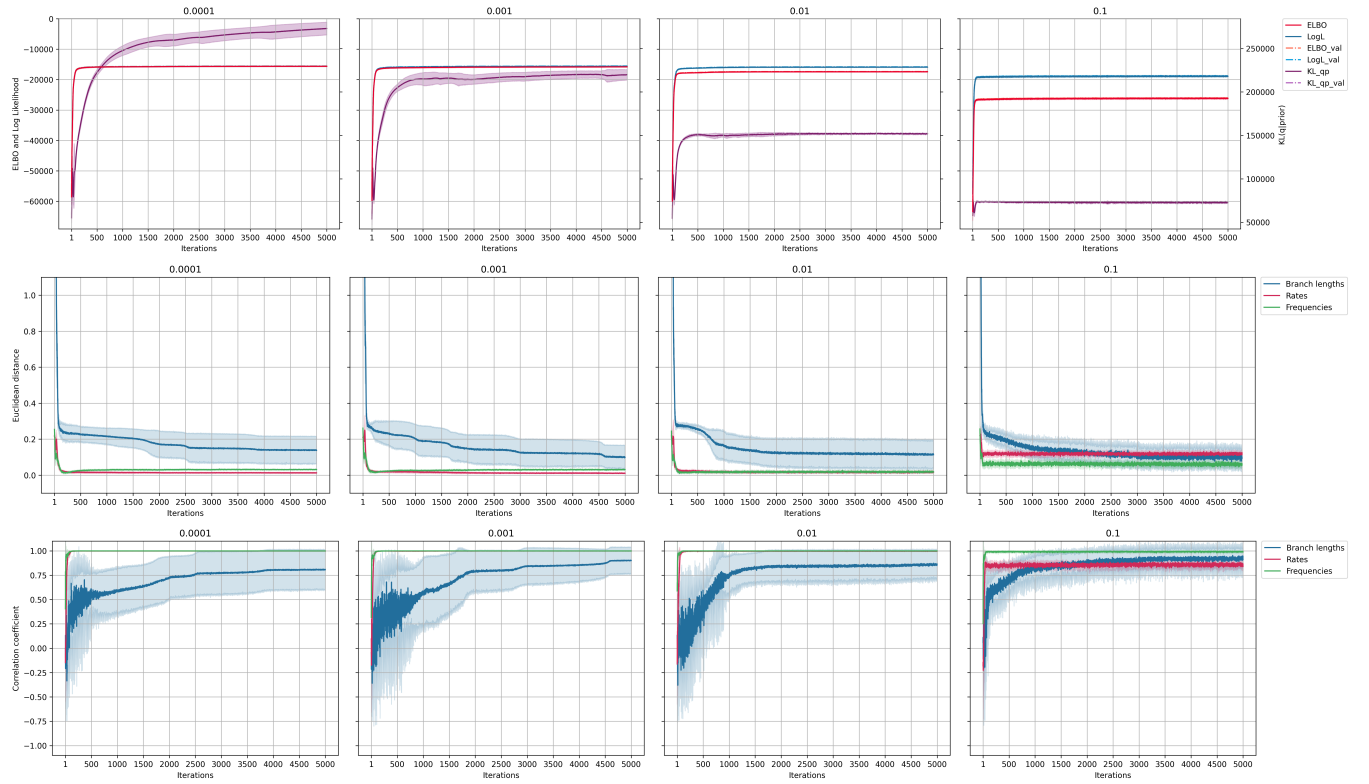


Figure 2: Convergence and performance of EvoVGM_GTR model for multiple settings of α_{KL} .

nucleotides. The sequence alignments used in the training step of the EvoVGM models were simulated with different random seeds from those used in the validation step but with the same array of evolutionary parameters.

Performance metrics. We report the results of the performance of EvoVGM models in terms of the ELBO, the Log Likelihood (LogL), and the KL divergence between the approximate densities and the priors (KL_qp) on the training and the validation sequence alignments. To assess the accuracy of the estimated branch lengths, substitution rates and relative frequencies, we compute the Euclidean distance and the Pearson correlation coefficient between their arrays and those of actual parameters used for alignment simulation. Finally, we show the ratio of its estimated and actual values for the κ parameter.

4.1 Hyper-Parameters Fine-tuning

First, we assessed the effects of different hyper-parameters on the convergence and the accuracy of the EvoVGM models to approximate the true distributions of the evolutionary parameters. For each hyper-parameters setting, the model was trained ten times, using different weight initialization, on the same alignment of five 5000-bp sequences. Based on the results of a grid search with different combinations of hyper-parameters, we defined the default components of the EvoVGM models which include a set of one-hidden-layer variational encoders with a hidden size of 32. We placed uniform

priors on ancestral states, substitution rates and relative frequencies, and independent gamma priors on branch lengths with a prior expectation of 0.1. Moreover, we used a 100-sample EvoVGM estimator with regularization coefficient α_{KL} equals 10^{-3} and Adam optimizer [14] for stochastic gradient ascent with learning rate of 0.005.

Figures 2, A.1 A.2 and A.3 highlight the performance of EvoVGM_GTR model (implementing a GTR substitution model) trained with multiple values of the coefficient α_{KL} , the size of the hidden layers, the sampling size, and the learning rate, respectively. In general, EvoVGM_GTR models converge faster when the α_{KL} coefficient is lower, and the number of hidden layers and the learning rate are larger. The sample size does not affect the overall convergence. However, a small sample size induces a substantial variance in the estimator.

4.2 Assessing Consistency on Simulated Alignments

Next, we analyzed the consistency and the effectiveness of the EvoVGM_GTR model on sequence alignments simulated with different sizes. The models was built using the same default configuration and the same hyper-parameters defined in the previous analysis. Figure 3 shows the accuracy of the model during the training in terms of Euclidean distances and correlation coefficients of the parameters estimated from multiple alignments of five sequences with lengths of 100 bp, 1000 bp and 5000 bp. Conversely, figure 4

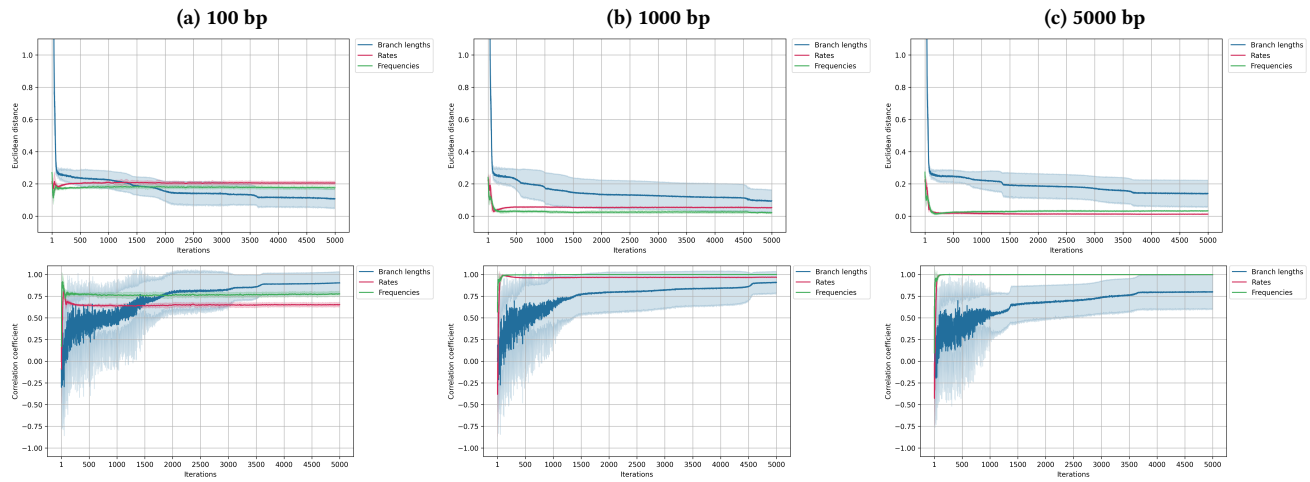


Figure 3: Performance of the EvoVGM_GTR model for multiple lengths of sequence alignments.

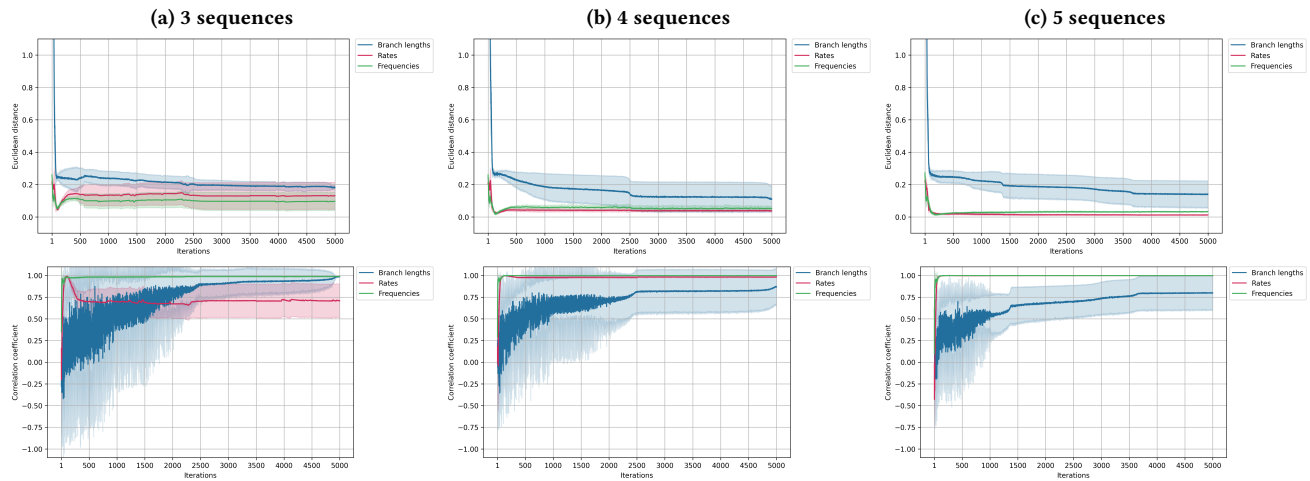


Figure 4: Performance of the EvoVGM_GTR model for multiple numbers of sequences.

shows the accuracy of the model in approximating the parameters on multiple alignments of lengths 5000 bp and with 3, 4 and 5 sequences. Usually, parameter approximation is improved when the number of sequences is higher and the alignments are longer. On the one hand, branch lengths suffer from high variance estimation and slow evolution at the beginning of the training across all sequences alignments. However, its variance and accuracy improve with more training iterations. On the other hand, the estimation of the substitution rates and the relative frequencies is more consistent with the ELBO and the LogL of the data, converges faster and has low variance with larger sequence alignments.

We present in tables 1, 2 and 3 the performance of trained EvoVGM_GTR models in approximating the evolutionary parameters from new multiple alignments, which were simulated with the same set of evolutionary parameters used in the training step. The estimated branch lengths are close and strongly correlated to their

actual values for all datasets except the smallest. EvoVGM_GTR estimates better relative frequencies than substitution rates in small datasets regarding the substitution model parameters. However, as the datasets get larger, the approximation of the substitution rates gets better.

Additionally, we evaluated the convergence and the accuracy of EvoVGM_JC69 and EvoVGM_K80, two variants of the EvoVGM model implementing JC69 and K80 substitution models, respectively. Each model was fitted ten times with different weight initialization on the exact sequence alignment. Figure 5 and table 4 show the results of the models trained and evaluated with alignments of five sequences of length 5000 bp. All models converge to values closer to or higher than the actual log likelihood of the data, which is calculated with equation 3 using the known ancestral sequences and evolutionary parameters. Moreover, they approximated the

Table 1: Distance and correlation between actual and estimated branch lengths by EvoVGM_GTR. Rows correspond to the number of sequences. Columns correspond to the alignment length.

	100			1000			5000		
	DIST	CORR	PVAL	DIST	CORR	PVAL	DIST	CORR	PVAL
3	0.300	0.984	0.114	0.090	0.980	0.126	0.097	0.986	0.107
4	0.076	0.994	0.006	0.086	0.998	0.002	0.085	0.992	0.008
5	0.081	0.986	0.002	0.069	0.995	0.000	0.116	0.962	0.009

Table 2: Distance and correlation between actual and estimated substitution rates by EvoVGM_GTR.

	100			1000			5000		
	DIST	CORR	PVAL	DIST	CORR	PVAL	DIST	CORR	PVAL
3	0.621	0.103	0.846	0.177	0.668	0.147	0.129	0.784	0.065
4	0.305	0.472	0.344	0.114	0.864	0.027	0.036	0.985	0.000
5	0.206	0.652	0.160	0.053	0.968	0.002	0.012	0.998	0.000

Table 3: Distance and correlation between actual and estimated relative frequencies by EvoVGM_GTR.

	100			1000			5000		
	DIST	CORR	PVAL	DIST	CORR	PVAL	DIST	CORR	PVAL
3	0.190	0.941	0.059	0.084	0.991	0.009	0.095	0.992	0.008
4	0.125	0.891	0.109	0.090	0.996	0.004	0.050	0.999	0.001
5	0.176	0.775	0.225	0.022	1.000	0.000	0.033	0.999	0.001

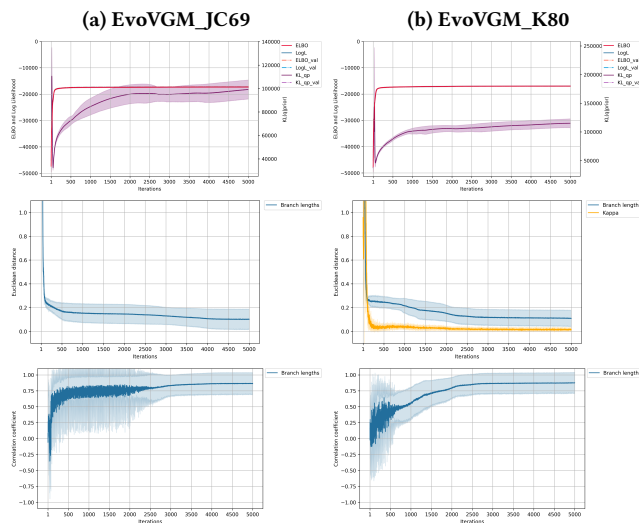


Figure 5: Performance of EvoVGM_JC69 and EvoVGM_K80.

branch lengths even when trained with datasets simulated with a different substitution model (Tables 1, A.1 and A.2).

4.3 Estimating Evolutionary Parameters on Real Alignment

Finally, we analyzed a real dataset to assess the robustness of the estimation provided by the variational generative model EvoVGM. The dataset was recovered from [20], and it consists of six sequences of Gene S of coronaviruses. We used the NGPhylogeny.fr platform [17] to build a multiple sequence alignment with MAFFT 7.407 [11]. The alignment has a length of 3688 bp after cleaning the sequences from gaps using Gblocks 0.91.1 [24].

We applied EvoVGM_GTR model to this dataset using the same configuration of variational encoders and hyper-parameters defined previously. We set gamma priors on branch lengths with a prior expectation of 0.01. We found that using α_{KL} with a value of 0.1 gives better estimations but with higher variance. We trained EvoVGM_GTR for 5000 iterations. Furthermore, we compared the estimations of EvoVGM_GTR model with those of MrBayes 3.2.7, a Bayesian phylogenetic inference program [8]. We ran MrBayes with four chains and two runs for one million iterations and sampling every 500 iterations.

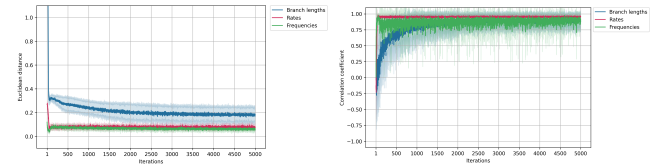


Figure 6: Comparison with MrBayes.

In figure 6, we show the evolution of the Euclidean distances and the correlation coefficients between the estimations of EvoVGM_GTR and those of MrBayes during the training. The estimations of the branch lengths differ from MrBayes estimations with a distance lower than 0.2 but with high variance. Furthermore, EvoVGM_GTR managed to estimate the substitution rates and the relative frequencies with low-variance values closer to the estimations of MrBayes.

5 DISCUSSION AND CONCLUSION

In this work we show that the variational Bayesian generative evolutionary model could constitute a viable approach to approximate the true parameters of an evolutionary model and generate associated sequence alignment. Our results can be summarized through three main observations: 1) all evoVGM models can perform well with an advantage over the evoVGM_GTR model; 2) in general, the models tend to have good performances for several configurations of hyper-parameters; 3) the model can generate alignment distribution fitting the properties of the learned one (data not shown here). Moreover, the evoVGM models provide an effective way of learning evolutionary model parameters for JC69, K80, and GTR. Their generalization to the other models such as HKY and Tamura-Nei is straightforward.

Table 4: Log likelihood estimates of EvoVGM models

	JC69		K80		GTR	
	MEAN	STD	MEAN	STD	MEAN	STD
REAL	-17249.830		-17024.340		-15818.739	
EvoVGM_JC69	-17209.913	142.128	-17287.278	185.441	-16491.810	125.664
EvoVGM_K80	-17203.100	151.758	-17007.724	133.294	-16495.530	175.024
EvoVGM_GTR	-17204.540	121.459	-17014.296	151.457	-15540.730	126.673

REFERENCES

- [1] Alan Amin, Eli N Weinstein, and Debora Marks. 2021. A generative nonparametric Bayesian model for whole genomes. In *Advances in Neural Information Processing Systems*, M. Ranzato, A. Beygelzimer, Y. Dauphin, P.S. Liang, and J. Wortman Vaughan (Eds.), Vol. 34. Curran Associates, Inc., 27798–27812.
- [2] David M Blei, Alp Kucukelbir, and Jon D McAuliffe. 2017. Variational inference: A review for statisticians. *Journal of the American statistical Association* 112, 518 (2017), 859–877.
- [3] Abdoulaye Banire Diallo, Vladimir Makarenkov, and Mathieu Blanchette. 2007. Exact and heuristic algorithms for the indel maximum likelihood problem. *Journal of Computational Biology* 14, 4 (2007), 446–461.
- [4] Gytis Dudas, Luiz Max Carvalho, Trevor Bedford, Andrew J Tatem, Guy Baele, Nuno R Faria, Daniel J Park, Jason T Ladner, Armando Arias, Danny Asogun, et al. 2017. Virus genomes reveal factors that spread and sustained the Ebola epidemic. *Nature* 544, 7650 (2017), 309–315.
- [5] Nuno R Faria, Andrew Rambaut, Marc A Suchard, Guy Baele, Trevor Bedford, Melissa J Ward, Andrew J Tatem, João D Sousa, Nimalan Arinaminpathy, Jacques Pépin, et al. 2014. The early spread and epidemic ignition of HIV-1 in human populations. *science* 346, 6205 (2014), 56–61.
- [6] Joseph Felsenstein. 1981. Evolutionary trees from DNA sequences: a maximum likelihood approach. *Journal of molecular evolution* 17, 6 (1981), 368–376.
- [7] John P. Huelsenbeck, Bret Larget, Richard E. Miller, and Fredrik Ronquist. 2002. Potential applications and pitfalls of Bayesian inference of phylogeny. *Systematic Biology* 51, 5 (2002), 673–688. <https://doi.org/10.1080/10635150290102366>
- [8] John P. Huelsenbeck and Fredrik Ronquist. 2001. MRBAYES: Bayesian inference of phylogenetic trees. *Bioinformatics* 17, 8 (2001), 754–755.
- [9] Michael I. Jordan, Zoubin Ghahramani, Tommi S. Jaakkola, and Lawrence K. Saul. 1999. An Introduction to Variational Methods for Graphical Models. *Machine Learning* 37, 2 (1999), 183–233. <https://doi.org/10.1023/A:1007665907178>
- [10] Thomas H Jukes and Charles R Cantor. 1969. Evolution of protein molecules. In *Mammalian protein metabolism*, H. H. Munro (Ed.), Vol. III. Academic Press, New York, 21–132.
- [11] Kazutaka Katoh and Daron M. Standley. 2013. MAFFT Multiple Sequence Alignment Software Version 7: Improvements in Performance and Usability. *Molecular Biology and Evolution* 30, 4 (01 2013), 772–780. <https://doi.org/10.1093/molbev/mst1010>
- [12] Andrew D Kern and David Haussler. 2010. A population genetic hidden Markov model for detecting genomic regions under selection. *Molecular biology and evolution* 27, 7 (2010), 1673–1685.
- [13] Motoo Kimura. 1980. A simple method for estimating evolutionary rates of base substitutions through comparative studies of nucleotide sequences. *Journal of molecular evolution* 16, 2 (1980), 111–120.
- [14] Diederik P. Kingma and Jimmy Ba. 2015. Adam: A Method for Stochastic Optimization. In *3rd International Conference on Learning Representations, ICLR 2015, San Diego, CA, USA, May 7–9, 2015, Conference Track Proceedings*, Yoshua Bengio and Yann LeCun (Eds.).
- [15] Diederik P Kingma and Max Welling. 2014. Auto-Encoding Variational Bayes. In *ICLR*. arXiv:1312.6114
- [16] Philippe Lemey, Marco Salemi, and Anne-Mieke Vandamme. 2009. *The phylogenetic handbook: a practical approach to phylogenetic analysis and hypothesis testing*. Cambridge University Press.
- [17] Frédéric Lemoine, Damien Correia, Vincent Lefort, Olivia Doppelt-Azeroual, Fabien Mareuil, Sarah Cohen-Boulakia, and Olivier Gascuel. 2019. NGPhylogeny.fr: new generation phylogenetic services for non-specialists. *Nucleic Acids Research* 47, W1 (04 2019), W260–W265. <https://doi.org/10.1093/nar/gkz303>
- [18] Adam Paszke, Sam Gross, Francisco Massa, Adam Lerer, James Bradbury, Gregory Chanan, Trevor Killeen, Zeming Lin, Natalia Gimelshein, Luca Antiga, Alban Desmaison, Andreas Kopf, Edward Yang, Zachary DeVito, Martin Raison, Alykhan Tejani, Sasank Chilamkurthy, Benoit Steiner, Lu Fang, Junjie Bai, and Soumith Chintala. 2019. PyTorch: An Imperative Style, High-Performance Deep Learning Library. In *Advances in Neural Information Processing Systems* 32, H. Wallach, H. Larochelle, A. Beygelzimer, F. d’Alchê-Buc, E. Fox, and R. Garnett (Eds.). Curran Associates, Inc., 8024–8035.
- [19] Danilo Jimenez Rezende, Shakir Mohamed, and Daan Wierstra. 2014. Stochastic backpropagation and approximate inference in deep generative models. *31st International Conference on Machine Learning, ICML 2014 4 (2014)*, 3057–3070. arXiv:1401.4082
- [20] Stéphane Samson, Étienne Lord, and Vladimir Makarenkov. 2022. SimPlot++: a Python application for representing sequence similarity and detecting recombination. *Bioinformatics* (04 2022). <https://doi.org/10.1093/bioinformatics/btac287> btac287.
- [21] David Sankoff and Mathieu Blanchette. 1999. Probability models for genome rearrangement and linear invariants for phylogenetic inference. In *Proceedings of the third annual international conference on Computational molecular biology*. 302–309.
- [22] Sam Sinai, Eric Kelsic, George M. Church, and Martin A. Nowak. 2017. Variational auto-encoding of protein sequences. In *NeurIPS 2017 Workshop on Machine Learning in Computational Biology*. 1–6. arXiv:1712.03346
- [23] Stephanie J. Spielman and Claus O. Wilke. 2015. Pyvolve: A Flexible Python Module for Simulating Sequences along Phylogenies. *PLOS ONE* 10, 9 (09 2015), 1–7. <https://doi.org/10.1371/journal.pone.0139047>
- [24] Gerard Talavera and Jose Castresana. 2007. Improvement of Phylogenies after Removing Divergent and Ambiguously Aligned Blocks from Protein Sequence Alignments. *Systematic Biology* 56, 4 (08 2007), 564–577. <https://doi.org/10.1080/10635150701472164>
- [25] Simon Tavaré et al. 1986. Some probabilistic and statistical problems in the analysis of DNA sequences. *Lectures on mathematics in the life sciences* 17, 2 (1986), 57–86.
- [26] Eli N Weinstein and Debora Marks. 2021. A structured observation distribution for generative biological sequence prediction and forecasting. In *International Conference on Machine Learning*. PMLR, 11068–11079.
- [27] Chris Whidden and Frederick A Matsen IV. 2015. Quantifying MCMC exploration of phylogenetic tree space. *Systematic biology* 64, 3 (2015), 472–491.
- [28] Ziheng Yang. 1994. Estimating the pattern of nucleotide substitution. *Journal of molecular evolution* 39, 1 (1994), 105–111.
- [29] Ziheng Yang. 2014. *Molecular evolution: a statistical approach*. Oxford University Press.
- [30] Ziheng Yang and Bruce Rannala. 1997. Bayesian phylogenetic inference using DNA sequences: a Markov Chain Monte Carlo method. *Molecular biology and evolution* 14, 7 (1997), 717–724.
- [31] Ke Yuan, Thomas Sakoparnig, Florian Markowitz, and Niko Beerenwinkel. 2015. BitPhylogeny: a probabilistic framework for reconstructing intra-tumor phylogenies. *Genome biology* 16, 1 (2015), 1–16.
- [32] Cheng Zhang and Frederick A. Matsen IV. 2019. Variational Bayesian Phylogenetic Inference. In *International Conference on Learning Representations*.

A APPENDIX

A.1 Development of the ELBO $\mathcal{L}(\phi, X)$

$$\begin{aligned}
\log p(X) &= \sum_{n=1}^N \log p(\mathbf{x}_n) \\
&= \sum_{n=1}^N \mathbb{E}_{q_\phi(\mathbf{a}_n, \mathbf{b}, \psi | \mathbf{x}_n)} \left[\log \frac{p(\mathbf{x}_n, \mathbf{a}_n, \mathbf{b}, \psi)}{p(\mathbf{a}_n, \mathbf{b}, \psi | \mathbf{x}_n)} \right] \\
&= \sum_{n=1}^N \mathbb{E}_{q_\phi(\mathbf{a}_n, \mathbf{b}, \psi | \mathbf{x}_n)} \left[\log \frac{p(\mathbf{x}_n, \mathbf{a}_n, \mathbf{b}, \psi)}{q_\phi(\mathbf{a}_n, \mathbf{b}, \psi | \mathbf{x}_n)} \frac{q_\phi(\mathbf{a}_n, \mathbf{b}, \psi | \mathbf{x}_n)}{p(\mathbf{a}_n, \mathbf{b}, \psi | \mathbf{x}_n)} \right] \\
&= \sum_{n=1}^N \mathbb{E}_{q_\phi} \left[\log \frac{p(\mathbf{x}_n, \mathbf{a}_n, \mathbf{b}, \psi)}{q_\phi(\mathbf{a}_n, \mathbf{b}, \psi | \mathbf{x}_n)} \right] + \mathbb{E}_{q_\phi} \left[\log \frac{q_\phi(\mathbf{a}_n, \mathbf{b}, \psi | \mathbf{x}_n)}{p(\mathbf{a}_n, \mathbf{b}, \psi | \mathbf{x}_n)} \right] \\
&= \underbrace{\sum_{n=1}^N \mathcal{L}_n(\phi, \mathbf{x}_n)}_{\geq \mathcal{L}(\phi, X)} + \sum_{n=1}^N \text{KL} \left(q_\phi(\mathbf{a}_n, \mathbf{b}, \psi | \mathbf{x}_n) \parallel p(\mathbf{a}_n, \mathbf{b}, \psi | \mathbf{x}_n) \right) \\
&\geq \mathcal{L}(\phi, X).
\end{aligned}$$

$$\begin{aligned}
\mathcal{L}(\phi, X) &= \sum_{n=1}^N \mathcal{L}_n(\phi, \mathbf{x}_n) \\
&= \sum_{n=1}^N \mathbb{E}_{q_\phi} \left[\log \frac{p(\mathbf{x}_n, \mathbf{a}_n, \mathbf{b}, \psi)}{q_\phi(\mathbf{a}_n, \mathbf{b}, \psi | \mathbf{x}_n)} \right] \\
&= \sum_{n=1}^N \mathbb{E}_{q_\phi} \left[\log p(\mathbf{x}_n | \mathbf{a}_n, \mathbf{b}, \psi) + \log p(\mathbf{a}) + \log p(\mathbf{b}) + \log p(\psi) \right. \\
&\quad \left. - \log q_{\phi_a}(\mathbf{a}_n | \mathbf{x}_n) - \log q_{\phi_b}(\mathbf{b}) - \log q_{\phi_\psi}(\psi) \right] \\
&= -N \left(\mathbb{E}_{q_\phi} \left[\log p(\psi) - \log q_{\phi_\psi}(\psi) \right] + \mathbb{E}_{q_\phi} \left[\log p(\mathbf{b}) - \log q_{\phi_b}(\mathbf{b}) \right] \right) \\
&\quad + \sum_{n=1}^N \mathbb{E}_{q_\phi} \left[\log p(\mathbf{x}_n | \mathbf{a}_n, \mathbf{b}, \psi) \right] + \mathbb{E}_{q_\phi} \left[\log p(\mathbf{a}) - \log q_{\phi_a}(\mathbf{a}_n | \mathbf{x}_n) \right] \\
&= -N \left(\text{KL}(q_{\phi_\psi}(\psi) \parallel p(\psi)) + \text{KL}(q_{\phi_b}(\mathbf{b}) \parallel p(\mathbf{b})) \right) \\
&\quad + \sum_{n=1}^N \mathbb{E}_{q_\phi} \left[\log p(\mathbf{x}_n | \mathbf{a}_n, \mathbf{b}, \psi) \right] - \text{KL}(q_{\phi_a}(\mathbf{a}_n | \mathbf{x}_n) \parallel p(\mathbf{a})) \\
&= -N \left(\text{KL}(q_{\phi_\psi}(\psi) \parallel p(\psi)) + \sum_{m=1}^M \text{KL}(q_{\phi_b}(\mathbf{b}^m) \parallel p(\mathbf{b})) \right) \\
&\quad + \sum_{n=1}^N \left(\frac{1}{L} \sum_{l=1}^L \sum_{m=1}^M \log p(\mathbf{x}_n^m | \mathbf{a}_n^l, \mathbf{b}^{m,l}, \psi^l) \right) - \text{KL}(q_{\phi_a}(\mathbf{a}_n | \mathbf{x}_n) \parallel p(\mathbf{a})).
\end{aligned}$$

A.2 Supplemental results

A.2.1 Branch length estimations of EvoVGM models.

Table A.1: Distance and correlation between actual and estimated branch lengths by EvoVGM_JC. Rows correspond to the number of sequences. Columns correspond to the alignment length.

	100			1000			5000		
	DIST	CORR	PVAL	DIST	CORR	PVAL	DIST	CORR	PVAL
3	0.129	0.969	0.160	0.069	0.982	0.121	0.143	0.982	0.120
4	0.166	0.938	0.062	0.065	0.997	0.003	0.079	0.997	0.003
5	0.179	0.841	0.074	0.096	0.993	0.001	0.076	0.990	0.001

Table A.2: Distance and correlation between actual and estimated branch lengths by EvoVGM_K80.

	100			1000			5000		
	DIST	CORR	PVAL	DIST	CORR	PVAL	DIST	CORR	PVAL
3	0.133	0.948	0.207	0.171	0.975	0.144	0.074	0.975	0.142
4	0.184	0.855	0.145	0.093	0.996	0.004	0.049	0.992	0.008
5	0.180	0.835	0.078	0.062	0.990	0.001	0.073	0.999	0.000

A.2.2 Hyper-parameters evaluation of EvoVGM models.

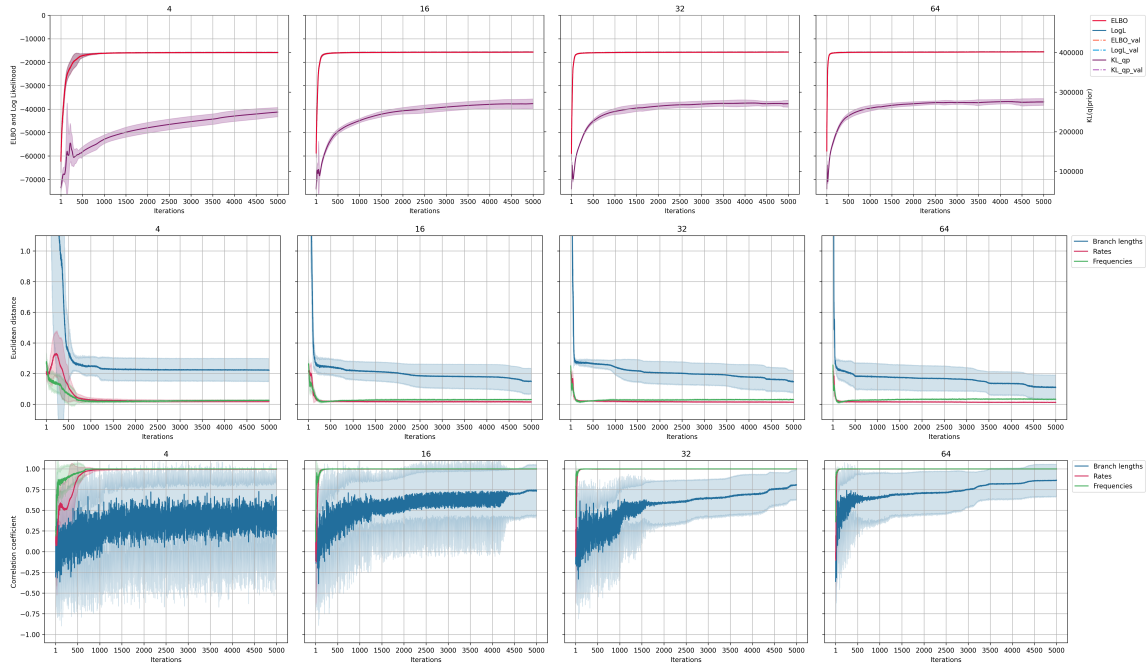


Figure A.1: Convergence and performance of EvoVGM_GTR model for multiple settings of the hidden size of the neural networks of the variational encoders.

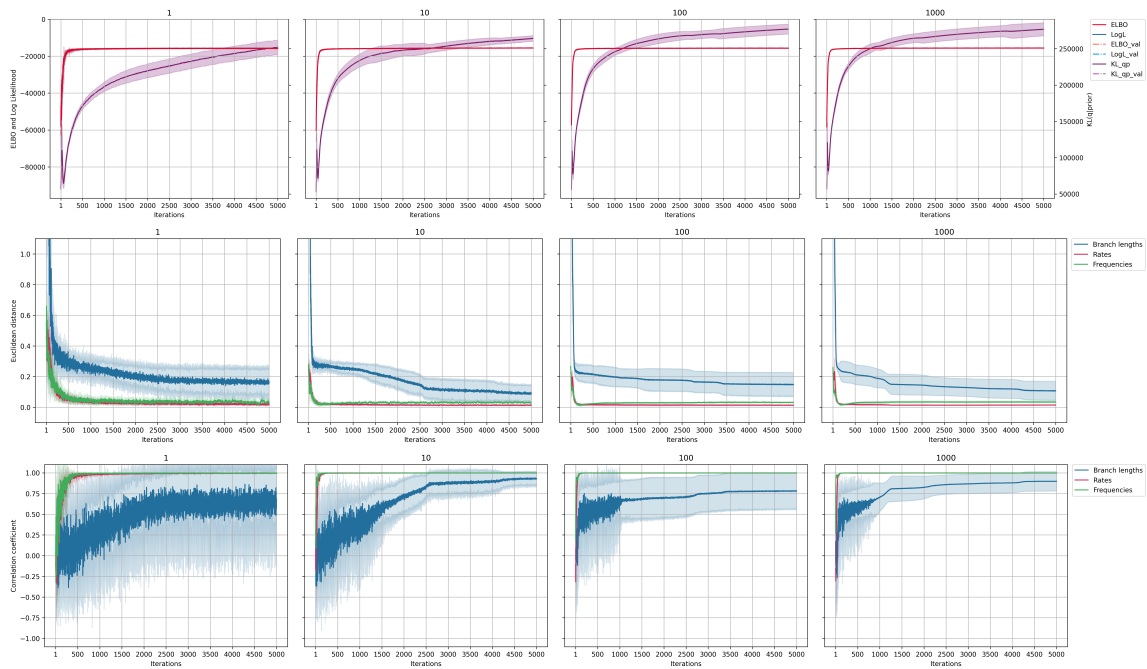


Figure A.2: Convergence and performance of EvoVGM_GTR model for multiple settings of the sample size.

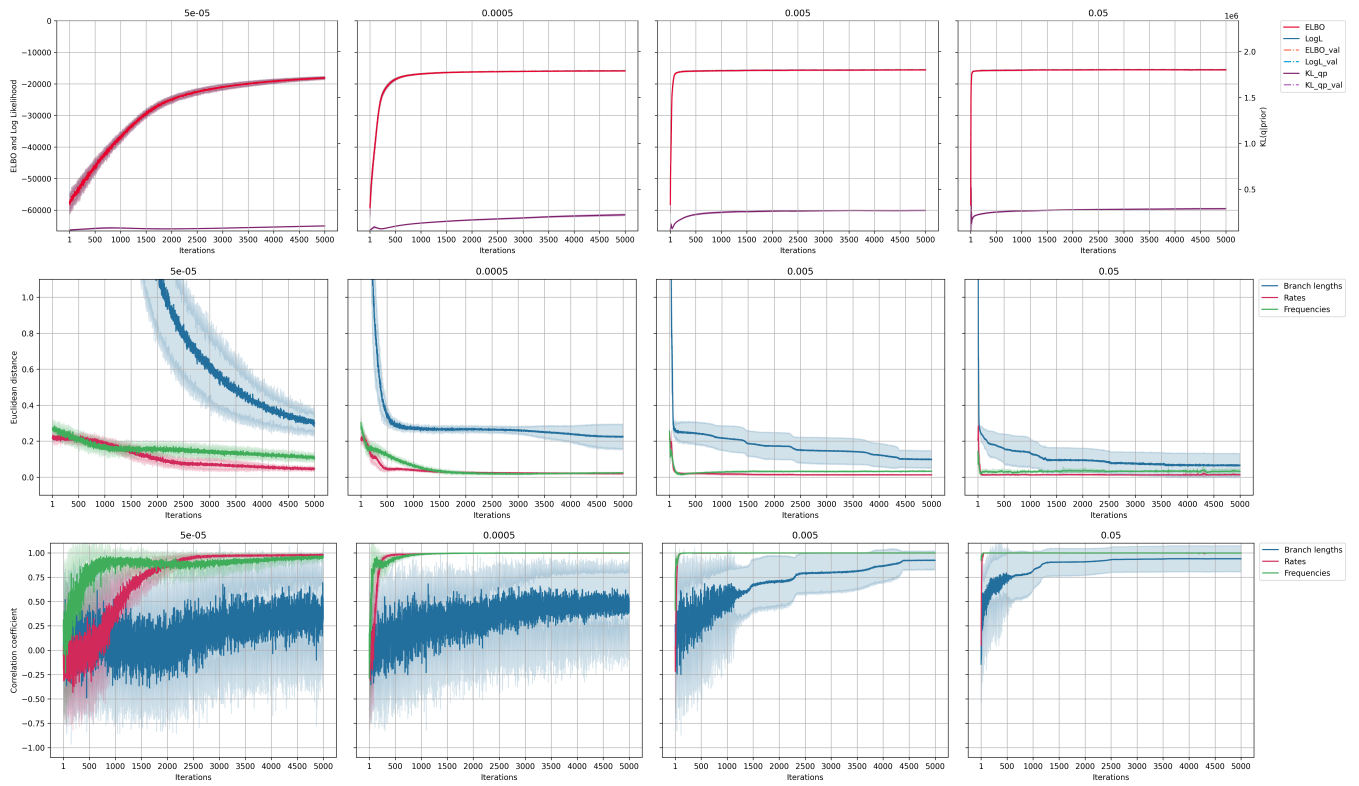


Figure A.3: Convergence and performance of EvoVGM_GTR model for multiple settings of the learning rate.